Adaptation to low temperatures of a DIC microscope with subnanometer sensitivity

Xavier Müller, Toshiya Kinoshita, Jacques Dupont-Roc

Adaptation to low temperatures of a DIC microscope with subnanometer sensitivity

X. Müller*, T. Kinoshita**, J. Dupont-Roc
Laboratoire Kastler Brossel†, Ecole Normale Supérieure,
24 rue Lhomond, F75231 Paris cedex 05, France
(November 12, 2000)

We show how a differential interference contrast (DIC) microscope can be adapted for low temperature operation by having only the microscope objective at low temperatures. The microscope body with delicate birefringent optics is kept at room temperature. A key part is the use of two Wollaston prisms with opposite anisotropic media to ensure a flat field. The device can detect optical path differences of the order of 10 pm/μm with a few second integration time. Images taken at several hour intervals can be subtracted, indicating a good mechanical stability.

I. INTRODUCTION

Differential interference contrast (DIC) microscopy is a powerful tool to reveal small phase objects or surface defects.[1,2] Microscope manufacturers provide apparatus which allow detection of sub-micron thick objects through color changes under white light illumination. Recent improvements have increased significantly the sensitivity of such apparatus up into the picometer range.[3–6] Such a sensitivity makes it worth to mention the advantages of this technique with respect to more recent ones such as scanning tunneling microscopy (STM) or atomic force microscopy (AFM). First it is a non scanning imaging technique providing all pixels in parallel. Second it is a remote sensing method. Only an optical window is necessary for observing inside a cell where special pressure, temperature or chemical conditions may be needed, and the sample is not submitted to mechanical perturbations. This is important for liquid films, which are sensitive to forces from a scanning tip. The lateral resolution is of course much lower than the scanning microscopes, a drawback compensated by a wider field. Some of these advantages are shared also by ellipsometric imaging which is widely used to study thin liquid films.[7–9] However the sensitivity reported for a true imaging apparatus,[8] about 5 nm, is significantly smaller and the field width is limited by the necessary inclination of the substrate.

As far as we know, DIC microscopy has been limited to room temperature observations for basic reasons that will be explained in section III. In this article, we report on how this technique can be adapted to observe inside a closed cell at liquid helium temperature. As an illustration, an image of the edge of a liquid helium film, a few tens nanometers thick, is presented.

II. FROM A DIC MICROSCOPE TO A HIGH SENSITIVITY PROFILOMETER

For the sake of clarity, the principle of the apparatus designed by Gleyzes *et al.*[3,6] is briefly summarized. It is based on a DIC microscope in a reflecting configuration[10] (Fig. 1, ignoring dash lines). Each point s of the light source L produces in the internal space of the microscope a nearly parallel light beam which is linearly polarized. It is split by a Wollaston prism W into two mutually coherent beams with linear polarizations at 45° from the initial one and perpendicular to each other. The angular separation between the two beams is small, on the order of 10^{-4} radian. They are focused by the microscope objective Obj on two close spots o_1 and o_2 on the observed surface (o_1o_2 is about the microscope resolution, 4 μm in our case). The corresponding return beams through the objective are re-combined by the same prism and are focused on the same point i of a CCD camera C (Dalsa CAD1 256×256 pixels). A phase plate introducing a phase difference ϕ_A between the two polarizations and a linear analyzer perpendicular to the initial polarizer act as a circular analyzer A. The phase ϕ_A and the phase difference ϕ_W introduced by the Wollaston prism add to the phase shift $2\delta(i)$ resulting from the surface elevation difference $Dz(i)$ at the points o_1 and o_2 which correspond to the point i of the image. $\delta(i)$ is related to $Dz(i)$ and to the light wavelength λ by

$$\delta(i) = 2\pi Dz(i)/\lambda \tag{2.1}$$

The light intensity detected at point i by the CCD camera may be expressed as

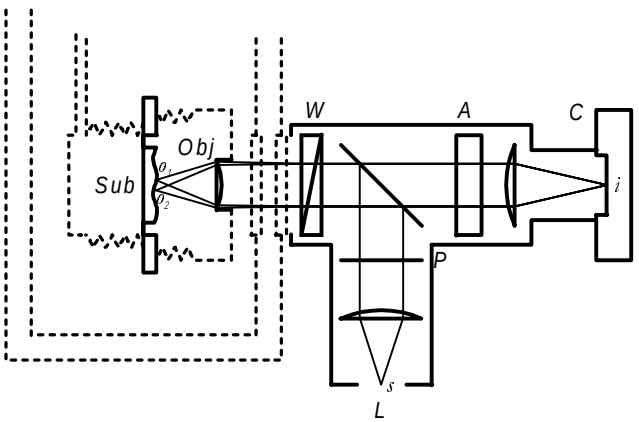

FIG. 1. The DIC microscope with phase modulation.[1,3–6] L: light source, P: linear polarizer, at 45° from the Wollaston axis, W: Wollaston prism, Obj: microscope objective, Sub: examined surface, C: CCD camera. The analyzer A is periodically switched between a σ^+ and σ^- configuration. From the two corresponding images, the elevation difference Dz at o_1 and o_2 is quantitatively computed. The dotted lines indicate how the cryostat is inserted into the microscope design.

$$I(i) = I_0 + I_m \sin^2 (\phi_A + \phi_W + 2\delta(i)) \tag{2.2}$$

I_m is the polarized light intensity. I_0 accounts for unpolarized light and CCD dark current. Both may possibly weakly depend on i due to non-uniformity of the illumination and of the CCD camera sensitivity. ϕ_A and ϕ_W should not depend on the incidence angle of the beam on the Wollaston prism and on the analyzer to ensure that they are both independent of i. The dependence of $I(i)$ on small differences $Dz(i)$ with interferometric sensitivity is the basis of the DIC microscopy.

Gleyzes *et al.* have brought important improvements by providing a true polarization detection, independent of light intensity, and an increased dynamical range. Two images are acquired for two opposite phases ϕ_A. They correspond to sums made in the memory of a PC of individual 8 bit images while switching ϕ_A at the video rate (33 images per second in our case). Summing two ensembles of 100 individual images provides two 16 bit images $I_+(i)$ and $I_-(i)$ in about a 6 s integration time. From these two images, a map of the circular polarization rate $\mathcal{P}(i)$ is computed:

$$\mathcal{P}(i) = \frac{I_+(i) - I_-(i)}{I_+(i) + I_-(i)} \tag{2.3}$$

The way ϕ_A is modulated in synchronism with the camera frame acquisition is described in references[3,6]. For the present purpose, it is sufficient to know that ϕ_A is modulated sinusoidally:

$$\phi_A = \phi_{Am} \sin\theta \tag{2.4}$$

and that $I_+(i)$ (resp. $I_-(i)$) corresponds to an average over $0 < \theta < \pi$ (resp. $-\pi < \theta < 0$). Then for each point i, the relation between the polarization $\mathcal{P}$ and Dz can be expressed through the variable

$$\psi(i) = \phi_W + 2\delta(i) \tag{2.5}$$

as

$$\mathcal{P}(i) = \frac{S \sin\psi(i)}{\frac{I_m+I_0}{I_m-I_0} - J_0 \cos\psi(i)} \tag{2.6}$$

where $J_0 = \mathrm{J}_0(\phi_{Am})$, $S = \frac{4}{\pi} \sum_{p\geq 0} \mathrm{J}_{2p+1}(\phi_{Am})/(2p+1)$ (the J's are Bessel functions). Typical values are $J_0 = 0.25$ and $S = 0.79$, known from the voltage driving the modulator. Once I_m and I_0 are determined by varying ϕ_W, the relation (2.6) can be inverted to compute $\delta(i)$, and thus to deduce $Dz(i)$, from $\mathcal{P}(i)$ (ϕ_W is usually set to zero). Note that $Dz(i)/o_1o_2$ is the local slope of the observed surface averaged over the microscope diffraction spot. Hence the apparatus is a quantitative profilometer and provides an image looking as a landscape with a side illumination. It can also be used to detect an additional dielectric layer (thickness h, refraction index n) on the initial surface. The corresponding optical phase shift is proportional to $(n-1)h$, for small h/λ. Through the DIC microscope, this phase shift of the return beam appears as a change in the substrate elevation h_A, named hereafter 'additional apparent height', which can be expressed as

$$h_A(i) = -\mathcal{S}(n-1)h(i) \tag{2.7}$$

The sensitivity factor $\mathcal{S}$ can be computed from the Fresnel law assuming flat interfaces. It lies between 0 and 2 depending on the substrate index of refraction. Subtraction of the initial image reveals the dielectric film only. An example will be shown below.

III. ADAPTATION TO LOW TEMPERATURE OPERATION

While integrating a complete interferometric imaging system at low temperature has been proved feasible,[11] it is here impossible because the Wollaston prisms cannot be cooled down due to highly anisotropic materials glued together. Having the entire microscope outside an optical cryostat is technically feasible, but this solution has several drawbacks. First the low temperature surface to be observed is necessarily separated from room temperature by several windows and a few centimeters. This long working distance practically limits the magnification of the microscope to less than 3 if the tube length of the microscope is kept constant. Furthermore thick flat windows between the object and the objective introduce spherical aberrations which have to be compensated for by a custom-made optical component. And finally the stability of the object at the bottom of the cryostat has to be achieved with respect to the outside microscope within better than its resolution. This is not an easy task because of the vibrations generated by bubbling cryogenic liquids and mechanical pumps. Recently it has been demonstrated that these drawbacks can be circumvented by a carefully designed long microscope.[12] It has not been used for DIC operation, but could probably be adapted for that purpose.

We have chosen another design in which the microscope is kept unmodified and outside the cryostat, except for the objective which is put inside, closely tied to the object to be observed. Hence, the cryostat windows are now in a section where the beams are parallel (dash lines in Figure 1), and introduce no optical aberration. Furthermore if the inner cryostat moves with respect to the outside part which holds the microscope body, this has little consequence because images are at infinity in the section between the objective and the Wollaston prism. The price to pay is that the objective and the focusing mechanism are at low temperatures. The original objective was replaced by a single aspherical lens (manufactured by *Thorlabs*, $f = 18.5$ mm, diameter 6 mm) giving a magnification 8.7 for the microscope. Shorter focal lengths are also available. This lens was used as the entrance window for the cell containing the sample surface. An indium seal was used to fasten it, as well as the other cryostat windows. The studied surface was fasten on a plate, the distance and the inclination of which can be adjusted through three fine pitch screws. They are acted on by rotating a stainless tube from room temperature. This tube can also be translated to be connected successively to each of the screws through a gear box and flexible steel cables. A fourth screw is used to translate the surface in front of the objective. The body of the microscope is fasten on the outer jacket of the cryostat in such a way that its optical axis can be aligned with the objective. This adjustment is however not critical, affecting only the amount of returned light, which of course has to be maximized to improve the signal to noise ratio. As the microscope objective is located further than it was in the original microscope design, the aperture diaphragm has to be shifted to remain conjugated with it.

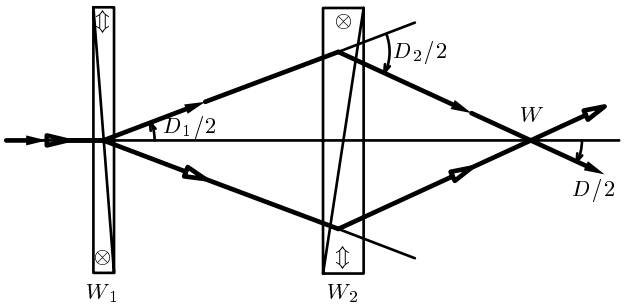

FIG. 2. Two Wollaston prisms, W_1 and W_2 with deviations D_1 and D_2, are equivalent to a unique one with deviation $D = D_1 + D_2$ located at the ray crossing point W (adapted from reference[2]). Rays with in-plane (resp. out of plane) polarization are labeled with filled (resp. empty) arrow heads. In the actual design $D_1 = 5.8 \times 10^{-4}$ rad, $D_2 = -7.8 \times 10^{-4}$ rad and the distance between W_1 and W_2 is 1 cm.

A critical element is the separating prism. For ϕ_W to be independent of the point i, the Wollaston prism has to be located at the image focus F' of the objective.[2] In the present case, this point is within the cryostat, making this condition impossible to meet. A well-known solution is to replace the Wollaston prism by a set of two such prisms W_1 and W_2 located further,[2] with deviations D_1 and D_2 such that the incoming central ray is divided into two rays which finally cross at W with the proper angle $D = D_1 + D_2$ (Fig. 2). This gives also the opportunity to use prisms made of materials with opposite anisotropy (one with $n_e - n_o > 0$ such as quartz, the other with $n_e - n_o < 0$ such as sapphire). This allows to make ϕ_W independent of the incidence angle up to third order,[13] providing a wider flat field. In order to avoid stray reflected light, the two prisms are tilted from the optical axis. The angles must be equal (resp. opposite) for the two prisms when using two opposite (resp. equal) anisotropic media. Two tuning displacements are allowed for the prisms. First, W_1 can be translated in its own plane producing a linear adjustment for ϕ_W. Second, the position of W_2 can be adjusted along the optical axis to make W and F' to coincide.

IV. RESULTS

The apparatus has been used to detect liquid helium films and meniscus on metallic surfaces (evaporated gold mirrors, or such surfaces covered by layers of cesium metal)[14,15]. Because liquid helium has a polarizability about one order of magnitude smaller than ordinary liquids ($n - 1 = 0.026$), it is much difficult to visualize thin helium films.

A. Image of a liquid helium film

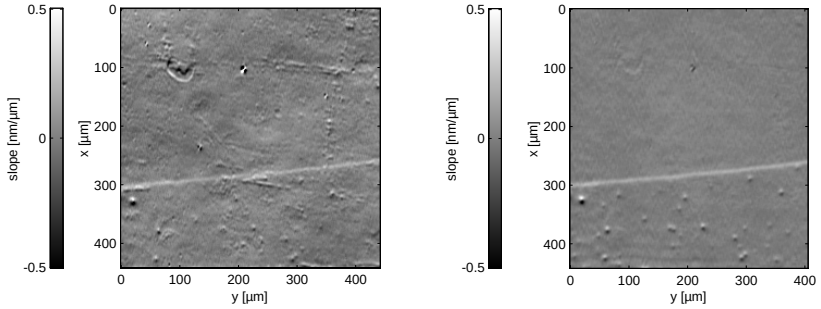

FIG. 3. (a) Image of a cesium metal surface partially wet by a helium film. The film edge appears as a white line superposed to the surface topography. (b) The image of the bare surface is subtracted from the previous image. Bumps visible in the lower part of the image are presumably due to local thickening of the film produced by submicronic dust grains.

Figure 3*a* is the image of a cesium metal surface partially wet by a helium film at 1.4 K. This situation is obtained by raising and then lowering the liquid meniscus on a vertical cesium mirror. The triple line remains pinned and a metastable film stays on the surface. Its thickness, about 50 nm, is determined by the compensation of the excess gravitational energy above the liquid film surface by the Van der Waals attraction of the metal surface. The film edge appears as a white line across the metal surface topography. The helium film is on the lower part of the picture. The gray scale is the local slope $Dz(i)/o_1o_2$. By subtracting to this image that of the same area taken before wetting, the image of the film edge can be extracted (see Figure 3*b*). Integration of the slope along a vertical line gives a profile of the corresponding apparent topography. An example is shown in Figure 4. The additional apparent height introduced by the film appears as a step -1.2 nm high, from which the film real thickness can be computed from formula 2.7 . The overall slope of the profile is due to a slight offset of W_2 along the optical axis from its ideal position which makes W and F' to coincide. The curvature comes from the residual variation of ϕ_W with the incidence angle. More details are available in reference[13,15]

B. Sensitivity

A simple way to measure the sensitivity of the profilometer is to subtract two pictures of the same area. Only a uniform noise remains, with a typical r.m.s. value for the slope about 14 pm/μm for a 6 s integration time, 40 pm/μm for 0.6 s. These values decrease when increasing the light power. However in order to avoid thermal perturbation of the sample, the light power was kept well below the saturation level of the CCD camera. Typical power reaching the sample was less than 10 μW, from which less than 10 percent was absorbed. Together with an integration time three times shorter, this weaker illumination may explain a sensitivity about six times worse than the room temperature value reported in reference[6].

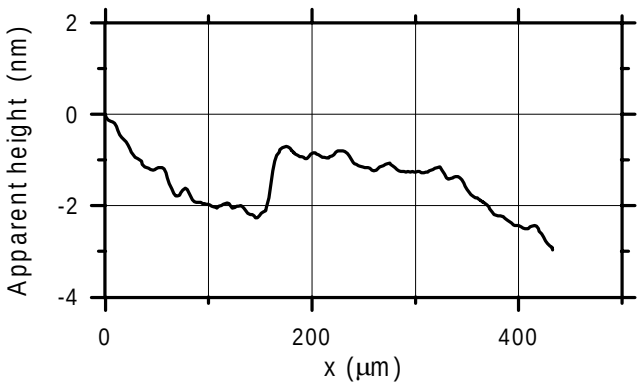

FIG. 4. Profile of the apparent surface topography. The edge of the 50 nm-thick liquid helium film appears as a step -1.2 nm high. The overall slope is meaningless (see text).

C. Stability

No blurring of the image was found while integrating over times as long as 8 s, indicating the absence of negative effects of the vibrations which are evidently present on the cryostat. Another interesting feature is the long term stability which determines the ability to perform image subtractions. When studying material deposited on the surface, one has to subtract the initial surface topography. Over several hours shifts between images are observed (which may come from either a shift of the camera or a translation of the substrate with respect to the microscope objective). Through interpolation between pixels, it is possible to find the translation which minimizes the sum over all pixels of the squares of the intensity differences between the two images. Typical translations are found to be 0.2 μm in the vertical direction and 1 μm in the horizontal one over 2 hours.[16] However the interpolation adds extra-noise which depends on the substrate roughness. For gold substrates with r.m.s roughness on the order of 200 pm (measured with the profilometer, which means over a characteristic distance of 4 μm), this interpolation noise is about 20 pm/μm. Hence for long lasting experiments, sensitivity is no more limited by the light power but by the interpolation noise.

D. Accuracy, Reliability

In formula (2.6), the signal Dz enters only through $\psi = \phi_W + 4\pi Dz/\lambda$. This allows an easy check of accuracy. As already mentioned, a translation of the prism W_1 produces a linear variation of ϕ_W. Thus if ϕ_A is kept to 0, a sinusoidal variation of $I(i)$ is obtained. Scanning an entire period gives the parameters I_m and I_0 of formula (2.6) and allow to calibrate the translation of W_1 versus ϕ_W. Hence one can produce a known variation $\delta\phi_W$, which amounts to an apparent change of the surface slope by $\lambda\delta\phi_W/4\pi o_1 o_2$. This value coincides within a few percent with the shift of the image gray scale produced by this additional slope. The correspondence between the measured slope and the surface true topography is nevertheless not so good, and requires some caution. First for the light wave, a metallic surface is equivalent to a perfect mirror located below the surface by one screening length. This penetration depth depends on the local complex refraction index of the metal. Furthermore coupling of the light wave to surface plasmons through surface roughness may add further phase shifts not related to surface topography. Both phenomena directly influence the sensitivity factor $\mathcal{S}$, and thus the apparent height h_A (see formula 2.7). From the Fresnel law applied to layered media, $\mathcal{S}$ varies between 0 and 2 depending on the penetration depth. Resonance with surface plasmons may cause $\mathcal{S}$ to reach larger values.[14] Hence optical properties of surface must be known for extracting quantitative information from surface images. If they are expected to be homogeneous, then the image indeed reflects the topography, within a constant factor $\mathcal{S}$ for additional transparent film.

ACKNOWLEDGMENTS

We are indebted to M. Lebec and A.C. Boccara for providing the design, electronics and software of the profilometer. We are grateful to them for their help and support.

* Present address : Centre de Physique Moléculaire Optique et Hertzienne, 351 cours de la libération, 33400 Talence, France.
** Present address : MIP Quantum Optics, München, Germany.
† Unité Mixte de Recherche 8852 de L'Ecole Normale Supérieure, de l'Université Pierre et Marie Curie, et du CNRS.
[1] See for instance M. Pluta, *Advanced light microscopy*, Elsevier (1989), or G. Roblin, in *Optique instrumentale*, P.Bouchareine editor, Les Editions de Physique (1996).
[2] M.G. Nomarski, *J. Physique et Radium* **16**, 9S (1955).
[3] P. Gleyzes, Thèse de l'Université Paris XI (1993) (unpublished).
[4] P. Gleyzes, A.C. Boccara, *J. of Optics* **26**, 251 (1995).
[5] M. Lebec, private com., (1996).
[6] P. Gleyzes, A. C. Boccara, H. Saint-Jalmes, *Optics Letters* **22**, 1529 (1997).
[7] L. Stilbert, T. Sandström, *J. Phys.* **44**, C10-79 (1983).
[8] D. Beaglehole, *Rev. Sci. Instrum.* **59**, 2557 (1988).
[9] M. Voue, J. De Coninck, S. Villette, M.P. Valignat, A.M. Cazabat, *Thin Solid Films* **313-314**, 819 (1998) and ref. in. F. Heslot, N. Fraysse, A.M. Cazabat, *Nature* **338**, 640 (1989).
[10] Actually in our case the BX30M model from *Olympus*.
[11] A.J. Manninen, J.P. Pekola, G.M. Kira, J.P. Ruutu, A. V. Babkin *Phys. Rev. Lett.* **69**, 2392 (1992).
[12] D. Douillet, E. Rolley, C. Guthmann, A. Prévost, *Physica* **B 284-288**, 2059 (2000).
[13] X. Müller, Thèse de l'Université Paris VI (1999) (unpublished).
[14] X. Müller, T. Kinoshita, J. Dupont-Roc, *J. Low Temp. Phys* **113**, 823 (1998).
[15] X. Müller, J. Dupont-Roc, *Physica* **B 284-288**, 143 (2000).
[16] The worse stability in the horizontal direction is related to a weaker mechanical guiding of the plate holding the sample to allow translation in this direction.